Hindawi
Journal of Nanomaterials
Volume 2022, Article ID 2867239, 12 pages
https://doi.org/10.1155/2022/2867239

Research Article

Mixed Interlaminar Fracture Toughness and Durability of Composites under Humid and Hot Conditions

Mingyong Li,[1] **Xia Meng**,[2] **and Qingyi Zhang**[3]

[1]*Department of Architectural Engineering, Shaoxing University Yuanpei College, Shaoxing 312000, China*
[2]*Gansu Institute of Earthquake and Seismic Engineering, Gansu Provincial Seismological Bureau, Lanzhou, 730000 Gansu, China*
[3]*Chengdu Branch of China Railway Scientific Research Institute Co., Ltd., Chengdu, 610000 Sichuan, China*

Correspondence should be addressed to Mingyong Li; 18767583669@usx.edu.cn

Received 22 March 2022; Revised 21 April 2022; Accepted 7 May 2022; Published 23 May 2022

Academic Editor: Awais Ahmed

Composite material is a new material prepared by several raw materials with different forms or properties through new processing methods. The composite not only maintains the advantages of the properties of each component but also can obtain the comprehensive properties that cannot be achieved by a single component through the complementarity and correlation of the properties of each component. The purpose of this paper is to study the effect of wet and hot conditions on the interlaminar fracture toughness and durability of composites. In this paper, the interlaminar fracture toughness and durability are studied, and the prediction and analysis method under wet and hot conditions is carried out. The effects of hot and humid conditions on interlaminar fracture toughness and durability were analyzed. The experimental results show that the longitudinal compressive strength of the unidirectional composite at 120°C and 1.00% moisture absorption is 29.53% lower than that at 20°C and 0.50% moisture absorption. Due to the high moisture absorption of aramid fiber, the longitudinal compressive strength of unidirectional aramid composite fiber will be significantly reduced in the humid and warm environment.

1. Introduction

Due to the special properties of nanomaterials, they are regarded as new materials in the 21st century. Advanced composites have been more and more used in aerospace and cycle fields because of their excellent properties, such as high special strength. The vulnerability and nonuniformity of the composite material itself make the failure of the hinge part of the composite material more complex, and the failure characteristics of the damage are also more complex. Its fracture performance is very different from that of metal materials. In addition, the connecting parts of composites are also very different. However, due to the complexity of composites and the continuous emergence of various new fibers and matrix materials, the influence of the humid and hot environment on the mechanical and fatigue properties of composites is not obvious. At present, there is no complete and accurate evaluation system.

Advanced composites are increasingly used in the main structures of aircraft and automobiles. Due to the low interlaminar strength, delamination is one of the most serious failure modes in composites and their structures. It is widely used in the cohesion model and virtual crack closure technology to predict the delamination of composites and their structures under tensile, compressive, or impact loads [1, 2]. Therefore, the interlaminar fracture toughness of composites is very important for the design and analysis of composites and their structures. Interlaminar fracture toughness is generally considered an inherent property of composites, which needs to be obtained by a delamination test. Therefore, it is very important to develop a simple and accurate test method to determine the interlaminar fracture toughness.

The innovations of this paper are as follows. (1) This paper combines damp-heat conditions with composites and introduces the relevant methods of interlaminar fracture toughness considering damp-heat conditions in detail. (2) In the face of hot and humid conditions, the fracture toughness and durability of composites are studied in this paper. By evaluating the experimental results and comparing the data

changes, it is concluded that the longitudinal compressive strength of unidirectional aramid composite fiber will be significantly reduced in the humid and hot environment.

2. Related Work

The influence of the environment is complex. For example, high temperature and moisture absorption will increase the plasticity of the matrix and increase the delamination toughness. On the other hand, it will cause microcracks in the matrix, will affect the bonding strength between the fiber matrix, may reduce the toughness, and will have different effects on different types of resins. Zhang et al. studied the effects of lime content, slag content, and moisture content on the thermal and wet properties of lime slag/soil composites by the response surface method and lime preparation process. The results showed that the lime content, slag content, and moisture content will affect the overall thermal and wet properties. Under the action of alkaline excitation and micro aggregate, the optimized lime slag/soil composite has the advantages of compact structure, reasonable mechanical properties, and comprehensive properties of heat and moisture. However, their data is less [3]. Zong et al. adopted the uniform experimental design and multiple nonlinear regression formula. They studied the Ce-La dose results (Ce-La molecular ratio and tetrabutyl titanate). The effects of the volume ratio of tetrabutyl titanium to tetraethyl orthosilicate on the hygroscopicity and photocatalytic properties of Ce-La/TiO_2 hollow microspheres were studied. The results show that these four factors have an effect on hygroscopicity. However, their research is not comprehensive enough [4]. Kasaragadda et al. applied superhydrophobic coatings to the surfaces of carbon, Kevlar, and glass fiber composites to eliminate the absorption of water by the composite structure. The test results show that when the composite surface is coated with a superhydrophobic coating, the moisture absorption is much smaller than that of the uncoated composite sample. However, their influencing factors are not single [5]. Yu et al. used the strong van der Waals force between superaligned carbon nanotubes (SACNT) to design a self-supporting 3D CNT/$CaCl_2$ radiator, which has better heat dissipation performance than aluminum fins. This high-efficiency refrigerator provides another heat management method for electronic products. However, their content is not novel enough [6]. Tanaka et al.'s study measured the specific volume and softening point of the resin by a single fiber drawing test at room temperature, 40°C, and 80°C. It was used to evaluate the fiber/matrix interface characteristics of the CF/PA9T composite model, and the results were compared with those of the CF/PA6 and CF/PA12 composite models. The resin expansion and interfacial shear strength of CF/PA9T model composites decreased with the increase in temperature, and the decreased range of interfacial shear strength of CF/PA9T model composites was less than that of CF/PA6 and CF/PA12 model composites. The reduction of high-temperature residual stress below 80°C does not cause chemical modification and softening of the resin but reduces the interfacial shear strength of the fiber matrix. However, their process is more complicated [7]. Liu et al. expanded its application in the electronics and membrane industry. It is aimed at developing radiation with heat resistance, conductivity, and moisture resistance by using PCT as the reactive reinforcement and applying the solid-state interface reaction (SSIR) between PCT and PA6. According to the results, SSIR occurred between PA6 and PCT. However, their research is not specific enough [8]. Chen et al. mixed natural corn starch with galactomannan (NS-GM) to produce the starch-galactomannan complex after wet heat treatment (HMT). They studied the in vitro digestibility and physicochemical properties of starch and starch-galactomannan complex. Their study found that the resistant starch content of HMT NS-GM composite granules was related to the galactose/mannose residue ratio of galactomannan. However, their conclusion is not comprehensive [9]. Han et al. synthesized a unique amino-functionalized metal-organic skeleton (sN-MIL) with a small pore size and low specific surface and developed a new heat-resistant and moisture-resistant bismaleimide (BD) resin with ultralow dielectric loss and high toughness. They discussed in depth the reasons behind these attractive properties of sN-MIL/BD composites. However, their content is not detailed enough [10].

3. Interlaminar Fracture Toughness Method considering Wet and Hot Conditions

3.1. Composites in Hot and Humid Conditions

3.1.1. Composite Material. Composite material is a new material prepared by several raw materials with different forms or properties through new processing methods. The new material processed and prepared by composite means has a clear interface between the organizational components in the material, which not only maintains some excellent characteristics of the original material components but also has superior characteristics that the original material components do not have. Composite materials include the matrix and reinforcement. Among them, the reinforcement plays an important role in bearing the external load in the composite, and the static properties of the composite are mainly determined by the characteristics of the reinforcement [11, 12].

The matrix of another main part of the composite mainly plays the role of coordination with the added solid. The solid added plays the role of supporting and fastening the solid added, and the load transfer between the solid added and the solid added protection. Matrix materials can also improve some properties of composites. In this paper, resin is selected as the base material because of its low density and ceramic as the die material because of its high-temperature resistance, and metal as the die material must obtain higher hardness and shear properties. As we all know, polymer matrix composites have another name in engineering applications, also known as resin matrix composites. In practical engineering applications, we use more thermoplastic resins and thermosetting resins. Among thermosetting resins, epoxy resin has the advantages of strong adhesion

and good corrosion resistance. It has been widely used in engineering applications, with good fiber surface permeability and convenient processing, preparation, hardening, and casting. Thermoplastic resin has good processability [13, 14]. Therefore, when the heating temperature reaches the transition temperature, they will soften again. Based on this excellent performance, it is easier to manufacture cast composites, and this resin has very good fracture resistance and high hardness. The drawback is that the coefficient of this resin is not high and the heat resistance is not very good.

3.1.2. Influence of the Damp and Hot Environment on Composites. During the use of composite materials, they will encounter the changing atmospheric environment. They will be used in nature with changing temperature T and relative humidity RH for a long time. When the natural environment's temperature and humidity are relatively high, water molecules may enter the polymer components and further diffuse. In view of the tiny cracks and gaps in the composite structure and the defects contained in the internal interface of the composite, the penetration rate and saturated moisture absorption rate of water in the material will be improved. The mechanical properties and electromagnetic properties of composites are bound to be greatly affected by them. In the end, the utilization efficiency of composites will be reduced and even the products will be damaged [15]. Water molecules penetrate into the tissue between the fiber and the matrix, causing the glue of these parts to lose viscosity and be transmitted to the fiber through the interface, resulting in fiber damage.

It is generally believed that glass fiber and carbon fiber do not absorb moisture, while aramid fiber has greater moisture absorption. It can be seen from Table 1 that the hygroscopicity of the glass fiber- and carbon fiber-reinforced composites is significantly lower than that of the resin matrix. The hygroscopicity of the aramid fiber-reinforced composites is four times that of the resin matrix. The phenomenon of water corrosion of glass fiber is found.

The influence of the liquid and warm environment on fiber-reinforced resin matrix composites is the synergistic effect of humidity and temperature, which is mainly due to the different degrees of damage to the resin matrix and the connection interface between reinforced fiber and resin/fiber. Heating can accelerate the moisture absorption rate, increase the moisture absorption balance of the material, and reduce the equilibrium time.

3.2. Fracture Mechanics Solution of Composite DCB. Due to the low interlaminar strength of laminates, delamination is the most common and main failure form.

From the point of view of mechanical fracture, separation belongs to the propagation behavior of the interlayer crack. According to the classification of cracks in fracture mechanics, their separation is mainly divided into three ways: I, II, and II, which depend on the stress at the edge of the crack. Type I separation, with the edge stress perpendicular to the crack surface, belongs to the open type. Type II separation, with the edge stress parallel to the crack surface, belongs to the shear type. Type III peeling, with the peak voltage on the crack surface perpendicular to the crack, tears in the propagation direction. In engineering practice, the stress state at the crack tip is often a complex stress state, which is the composite of the three basic types [16, 17].

Table 1: Water absorption of the material after immersion in water for 7 days (10^{-2} g/cm^3).

Material temperature	22°C	60°C	100°C
Epoxy resin	0.24	0.39	1.12
Glass fiber-reinforced composites	0.13	0.24	0.68
Carbon fiber-reinforced composites	0.24	0.33	0.82
Aramid fiber-reinforced composites	0.48	0.68	4.78

3.2.1. Griffith's Energy Release Rate. According to Griffith's law, the energy release rate refers to the energy consumed per unit of the newly generated surface area during fracture, as shown in Figure 1.

The mathematical form of the energy release rate can be expressed as follows:

$$G = \frac{\delta \prod}{\delta M} = \frac{\delta(W-U)}{\delta M} = \frac{1}{N} \cdot \frac{\delta(W-U)}{\delta m}, \quad (1)$$

where u represents the total strain energy, w represents the external force work, M represents the surface area of the newly generated crack surface, n represents the specimen width, and DM is the crack growth increment. Using the following relationship: $C = \varepsilon/P$, $W = P\varepsilon$, and $U = 1/2P\varepsilon$, formula (1) can be transformed into the following form:

$$G = \frac{1}{2N} P^2 \frac{\delta C}{\delta m}, \quad (2)$$

where P and ε are the applied load and opening displacement, respectively. C represents the flexibility of the DCB specimen.

3.2.2. Fracture Mechanics Solution Based on the Beam Theory. The energy release rate of the DCB sample shown in Figure 2 can be analyzed by the basic beam theory.

According to Euler's beam theory, the opening displacement of DCB sample δ and the force P applied at both ends have the following relationship:

$$\varepsilon = \frac{2Pm^3}{3E_{xx}A}, \quad (3)$$

where E_{xx} represents the elastic modulus of the sample along the fiber direction, M represents the crack length, h is the thickness of the single cantilever beam, a represents the section moment of inertia of the single cantilever beam, and $A = 1/12Nh^3$.

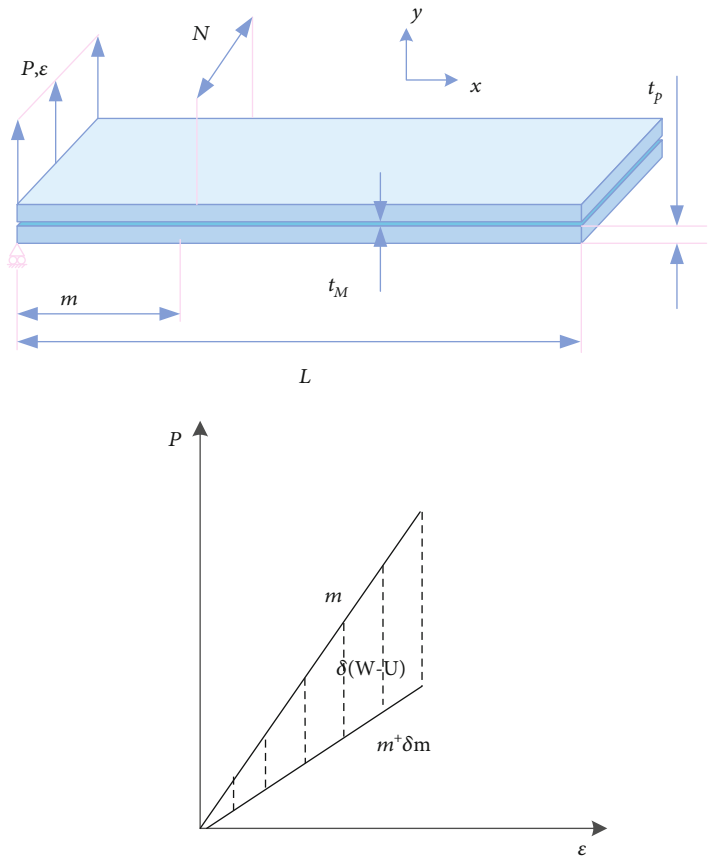

Figure 1: Schematic diagram of Griffith's energy release rate.

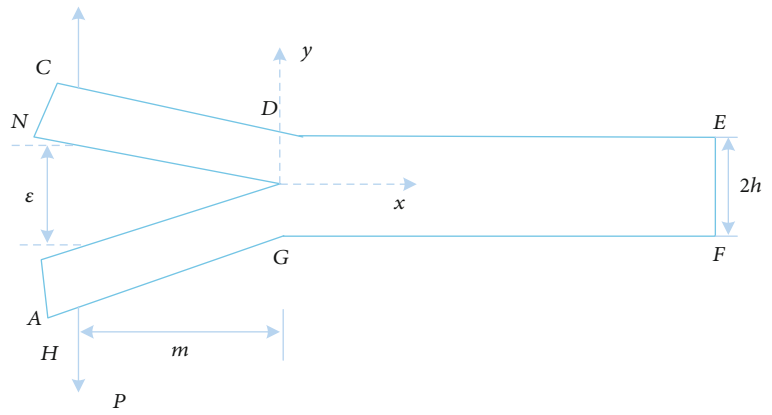

Figure 2: DCB sample.

By introducing formula (3) into formula (2), the expression of the energy release rate based on Euler's beam theory can be obtained:

$$G = \frac{1}{N} \cdot \frac{P^2 m^3}{3E_{xx}A}. \tag{4}$$

Using formula (3) and its transformation form, the energy release rate G in formula (4) can be rewritten as follows:

$$G = \frac{9E_{xx}A \cdot \varepsilon^2}{4Nm^4}, \tag{5}$$

$$G = \frac{3P\varepsilon}{2Nm}, \tag{6}$$

$$G = \frac{1}{N} \cdot \sqrt{\frac{9P^4 \cdot \varepsilon^2}{4E_{xx}A}}. \tag{7}$$

Theoretically, the energy release rate calculated by formulas (4)–(7) should be the same. However, if the load and displacement obtained from the finite element are used and the energy release rate is calculated by the four formulas, the accuracy of their results is different. The reason is that the load-displacement relationship of the DCB sample given in formula (3) is an approximate solution.

3.2.3. Two-Dimensional Elastic Solution. Formula (3) introduces some simplified assumptions when calculating the load-displacement relationship of the DCB sample: the energy in the DCB sample is only stored in arms ABCD and AIHG. As shown in Figure 2, strain energy is also stored in the noncracked region DEFG, but this is not considered in formula (3). In addition, the uncracked region is deformed and not completely rigid as required by the simple cantilever theory. Therefore, formula (3) used to calculate the load-displacement relationship of the DCB sample is inaccurate [18]. In order to overcome the shortcomings of the simple beam model, the researchers used the orthogonal scaling method and finite element analysis (FEA) to give the solution of the energy release rate of the two-dimensional orthotropic DCB:

$$G = \frac{P^2 m^2}{N \cdot E_{xx}A}\left(1 + 2\alpha\frac{h}{m} + \alpha^2\frac{h^2}{m^2}\right), \tag{8}$$

where

$$\alpha = \left[0.677 + 0.146(\beta\text{-}1) - 0.0178(\beta\text{-}1)^2 + 0.00242(\beta\text{-}1)^3\right] \cdot \left(\frac{E_{yy}}{E_{xx}}\right)^{-1/4}, \tag{9}$$

$$\left(\frac{E_{yy}}{E_{xx}}\right)^{-1/4}\beta = \frac{\sqrt{E_{xx}E_{yy}}}{2G_{xy}} - \sqrt{\nu_{xy}E_{yx}}. \tag{10}$$

E_{xx}, E_{yy} and G_{xy} are Young's modulus and the shear modulus, respectively; ν_{xy} and ν_{yx} are Poisson's ratios. For isotropic materials, $\beta = 1$ and $\alpha == 0.677$, which is consistent with the two-dimensional elastic solution of isotropic DCB. For the case of $M/H \gg 1$, the energy release rate given by formula (8) is very close to that obtained by formula (4) based on the simple beam theory.

3.2.4. Finite Element and Verification. A two-dimensional finite element model is established to verify the accuracy of formulas (4)–(8) in calculating the energy release rate of orthotropic DCB. The boundary conditions of the finite element model are shown in Figure 3, in which the lower left hinge point is fixed ($u_x = u_y = 0$), and the concentrated force P is applied at the upper left point. The mechanical properties of the composites used in the finite element model are as follows: $E_{xx} = 110$ GPa, $E_{xx} = E_{yy} = 8.07$ GPa, $G_{xy} = G_{xz} = 3.79$ GPa, $G_{yz} = 3.28$ GPa, $\nu_{xy} = \nu_{xz} = 0.32$, and $\nu_{yz} = 0.45$. Through the linear elastic finite element analysis, the opening displacement required to calculate the energy release rate in formulas (5)–(7) is obtained. It is difficult to obtain the solution of $x = -2$ at the point of $y = -H$, because it is difficult to obtain the singularity of the displacement at the point of $y = -M$.

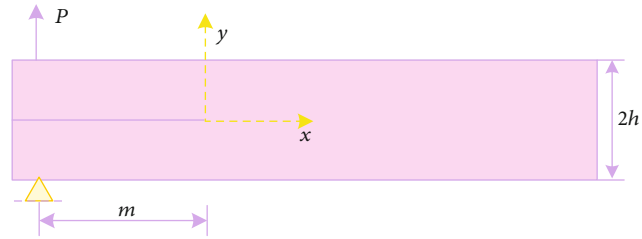

Figure 3: Finite element model network planning and boundary conditions.

3.3. Double Flexibility Method for Determining Interlaminar Fracture Toughness

3.3.1. Method Overview. It can be seen from Figure 3 that most solutions of Euler's beam theory (except formula (7)) are not accurate enough when actually calculating the energy release rate of the DCB sample. Therefore, these formulas need to be modified before they can be used. The researchers studied the complex deformation of the crack edge and proposed the concept of equivalent crack length $m_{\text{eff}} = m + \Delta$, i.e., modified beam theory (MBT), whose compliance type can be expressed as follows:

$$C = \frac{8(m + \Delta)^3}{E_{xx}Nh^3}. \tag{11}$$

E_{xx} is Young's modulus, and H is the thickness of the single cantilever beam.

According to the ASTM standard, the Δ can be assured. The linear regression method is used to linearly adjust the compliance cube root $C^{1/3}$ related to the crack length M. The intersection of the straight line and the M axis is m, as shown in Figure 4.

By replacing formula (11) with formula (2) and through appropriate transformation, the formula of the critical energy release rate is as follows:

$$C_{\text{AC}} = \frac{3P\varepsilon}{2N(m + |\Delta|)}. \tag{12}$$

Similarly, the flexibility calibration method (CC) and the modified flexibility calibration method (MCC) can also correct the flexibility. The flexibility expressions are formulas (13) and (14), respectively:

$$C = Mm^r, \tag{13}$$

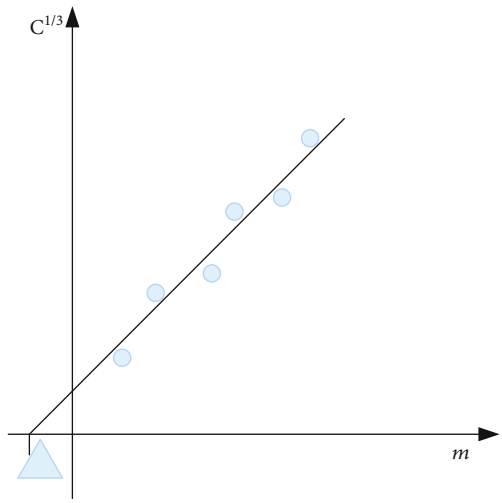

Figure 4: Modified beam theory.

$$C = \frac{1}{M_1^3}\left(\frac{m}{h} - M_2\right)^3. \tag{14}$$

Among them, R and M_1 are also obtained by the linear regression adjustment method similar to Δ. By introducing formulas (13) and (14) into formula (2), respectively, the corresponding expression of the critical energy release rate can be obtained:

$$G_{AC} = \frac{rP\varepsilon}{2Nm}, \tag{15}$$

$$C_{AC} = \frac{3P^2C^{2/3}}{2M_1Nh}. \tag{16}$$

According to formulas (12), (15), and (16), the three methods proposed by ASTM must record the crack propagation length and the corresponding force and displacement and determine the correction coefficients a, R, and M_1 in real time. This process is troublesome, and if tested in the high- and low-temperature environment, the method of the ASTM standard will be very difficult to achieve. Based on the contents, we propose a double flexibility method for the fracture resistance of composite DCB specimens without real-time recording of the crack length.

3.3.2. Theory of the Double Flexibility Method. In fact, if there is a highly accurate relationship between the applied load P, the crack length m, and the opening displacement ε , it is not necessary to measure the crack length, the applied load, and its corresponding displacement at the same time. In this paper, a high-precision relationship between force-displacement-crack length is established by using the solution of the high-precision energy release rate given by predecessors [19]. In this paper, the energy release rate solution formula (8) obtained from the two-dimensional elastic analysis is adopted, and formula (8) is brought into formula (2) for indefinite integration. The relationship between the applied load P and the displacement ε of orthotropic DCB can be obtained as follows:

$$C = \frac{\varepsilon}{P} = \frac{24}{NE_{xx}}\left(\frac{m^3}{3h^3} + \alpha\frac{m^2}{h^2} + \alpha^2\frac{m}{h}\right). \tag{17}$$

In this paper, the finite element model is used to verify the accuracy of formulas (3) and (17) in calculating DCB flexibility. When m/h is not used, the relative difference between formulas (3) and (17) and the finite element results are shown in Figure 5. It can be seen that formula (3) obtained from Euler's beam theory is too simple to calculate the flexibility of DCB, but the flexibility formula (17) obtained by integration is quite accurate.

For isotropic DCB, α is a constant value, equal to 0.677. Therefore, Young's modulus E_{xx} required in formula (7) can be obtained by the following method: the DCB test is conducted to obtain the force-displacement curve of the linear elastic loading section so as to obtain the DCB flexibility under the initial crack, which is brought into formula (17) to finally determine Young's modulus E_{xx}. After E_{xx} is determined, the fracture toughness of isotropic DCB can be calculated directly from formula (7) without measuring the crack length.

For anisotropic DCB, E_{xx} and α are unknowns. In order to determine these two parameters, a double flexibility method is proposed in this paper; that is, the flexibility C_0 loaded in the DCB test curve and the flexibility C_1 unloaded are used. The crack lengths corresponding to flexibility C_0 and C_1 are m_0 and m_1, respectively, which can be easily obtained by ultrasonic M-scan. It brings the two groups of crack lengths and corresponding flexibility into formula (17) to obtain the following:

$$C_0N = \frac{24}{E_{xx}}\left(\frac{{m_0}^3}{3h^3} + \alpha\frac{{m_0}^2}{h^2} + \alpha^2\frac{m_0}{h}\right), \tag{18}$$

$$C_1N = \frac{24}{E_{xx}}\left(\frac{{m_1}^3}{3h^3} + \alpha\frac{{m_1}^2}{h^2} + \alpha^2\frac{m_1}{h}\right). \tag{19}$$

It takes into account α as a positive number, where α and E_{xx} are as follows:

$$\alpha = \frac{-Y - \sqrt{Y^2 - 4XZ}}{2X}, \tag{20}$$

$$E_{xx} = \frac{24}{NC_1}\left(\frac{{m_1}^3}{3h^3} + \alpha\frac{{m_1}^2}{h^2} + \alpha^2\frac{m_1}{h}\right), \tag{21}$$

where

$$\begin{aligned} X &= \frac{m_1}{h}C_0 - \frac{m_1}{h}C_1, \\ Y &= \frac{{m_1}^2}{h^2}C_0 - \frac{{m_0}^2}{h^2}C_1, \\ Z &= \frac{{m_1}^3}{3h^3}C_0 - \frac{{m_0}^3}{3h^3}C_1. \end{aligned} \tag{22}$$

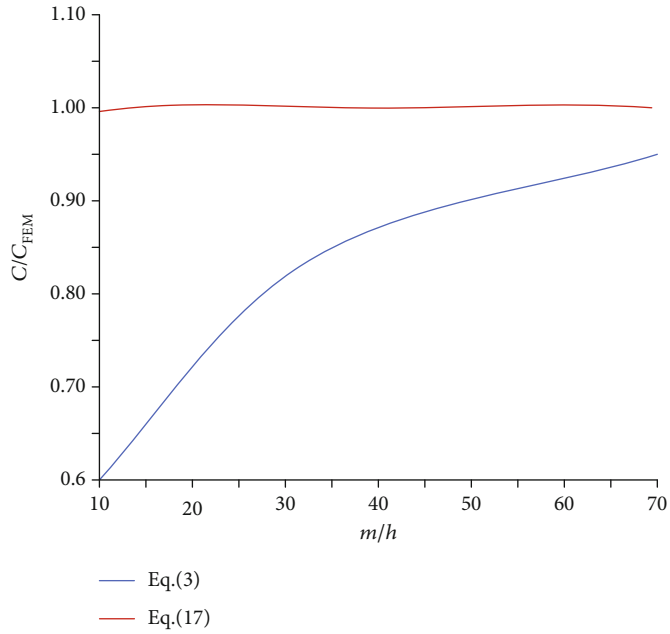

Figure 5: Formulas (3) and (17) calculate the relative difference between the botulinum toxin and finite element results.

Table 2: Composite material performance.

Material			Compound material			
Stretch	Strength (MPa)	84.76	Impact strength (kgcm/cm^2)	14.0	Glass transition temperature T_g (°C)	218
	Modulus (GPa)	3.29				
	Elongation at break (%)	3.34			Heat distortion temperature (°C)	198
Compression	Strength (MPa)	167.18			Density ρ (g/cm^2)	1.256
Bending	Strength (MPa)	134.47	Fracture toughness GIC (J/m^2)	95		
	Modulus (GPa)	3.66			Saturated moisture absorption in boiling water (%)	3.3

After determining α and E_{xx}, determine the relationship between flexibility C and crack length M. Using formula (17), the crack length m can be expressed as follows:

$$m = \sqrt[3]{\alpha^3 + \frac{\varepsilon N E_{xx}}{8P}} \cdot h - \alpha h. \tag{23}$$

That is, when the P force and ε displacement are known, the crack length can be calculated without additional measurement.

By introducing formula (23) into formula (8), the expression of the energy release rate without the crack length can be obtained:

$$G = \frac{P^2 h^2 \left(\alpha^3 + \left(\varepsilon N E_{xx}/8P\right)\right)^{2/3}}{N E_{xx} A}. \tag{24}$$

The significance of the formula is that the crack propagation length and fracture strength can only determine the duration of the test procedure from the force and displacement information during the test. It avoids measuring the crack propagation length during the test and makes it suitable for the hardness test environmental conditions of the type I interlayer under test conditions, such as low temperature [20, 21].

4. Experiment and Analysis of Interlaminar Fracture Toughness and Durability in the Humid and Hot Environment

4.1. Interlaminar Fracture Toughness Test

4.1.1. Materials. In this study, the hardness and heat resistance of the composite used are relatively good, and some of its main properties are shown in Table 2.

All the 24 ply unidirectional plates used in the test are about 4 mm thick. The cut specimen is 165 mm long and 30 mm wide. In one section of the test piece, a layer of Teflon film with a length of about 35 mm is prepaved in the middle layer as a prefabricated layer. The shape and geometric dimensions of the test piece are shown in Figure 6. After cutting, the test piece shall be dried and hygroscopic.

4.1.2. Load-Displacement Curve. Under normal temperature and dry conditions, the typical load-displacement curve of

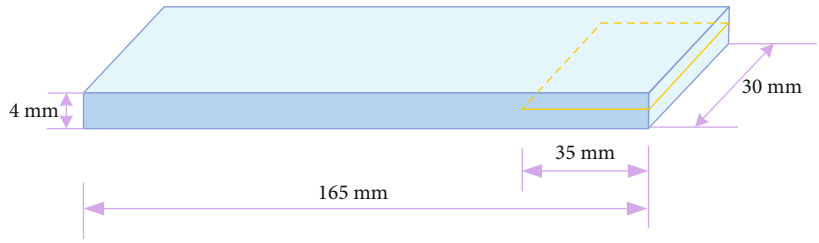

Figure 6: Shape and size of the test piece.

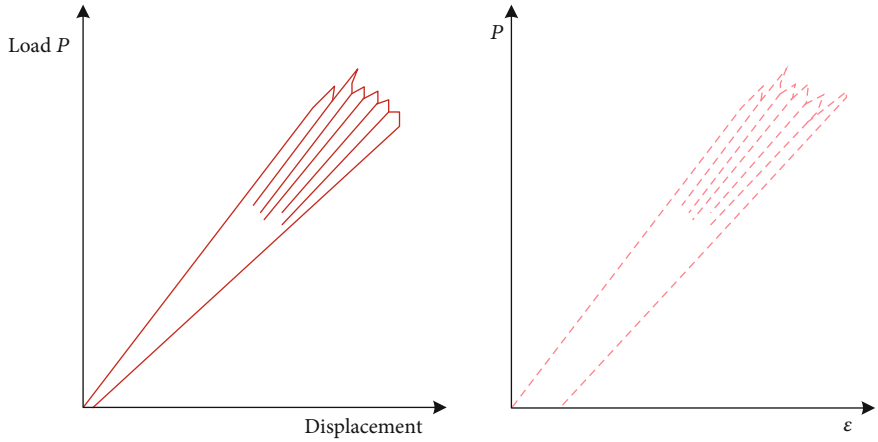

(a) Load-displacement curve of the MMF test under the normal temperature and dry state

(b) Test load-displacement curve with moisture absorption of 1.15% at 120°C

Figure 7: Comparison diagram of the load-displacement curve of the MMF specimen test.

the hybrid test is shown in Figure 7(a). Before crack propagation, the load-displacement curve is linear. When the crack propagates, it enters the nonlinear section. This is because the crack propagates, the crack length m increases, the stiffness of the beam decreases, the load-displacement curve of the crack propagation thickness is different from that before the crack propagation, and the slope of the straight-line section of the unloading curve decreases. In this environment, the unloading line is always straight and points to the origin. It can be seen that the linear relationship is established and there is no permanent deformation. It can be inferred that there is no plastic deformation problem [22]. In fact, from the shape of the unloaded specimen, there is no residual deformation.

In the high-temperature and high-humidity environment, the load-displacement curve of the MMF specimen has entered the nonlinear response section before crack propagation. This is most prominent in the test at 120°C and 1.15%, as shown in Figure 7(b). It is inferred that there is a certain plastic deformation at the tip of the crack before the crack propagation, and the crack propagates only after the plastic deformation. In terms of mechanism, the glass transition temperature of the interlayer resin decreases at high temperature after moisture absorption. The ambient temperature is very close to the glass transition temperature of the material after moisture absorption [23]. With the increase of material fluidity and high stress at the crack tip, plastic flow and plastic deformation easily occur. From the test piece after the test, there is indeed permanent deformation.

In addition, the unstable propagation of cracks can be observed during the test.

It can be seen from the load-displacement curve that in the initial stage of crack propagation, when the crack is small, the load increases with the increase of crack length, and the crack propagation is steady; in the later stage of crack propagation, the crack is long. Under the displacement loading mode, the load decreases and the propagation belongs to an unsteady state.

4.1.3. Fracture Failure Criterion. According to the test results, the type I and type II component values of pure type I and type II interlaminar fracture toughness and mixed type interlaminar fracture toughness are calculated by using the previous calculation formula. The criterion of crack (delamination) propagation under the complex load can be traced, and the scatter diagram of G_I-G_{II} can be made. The pure type I action state is regarded as the special state of G_{IIa}, and the pure type II action state is regarded as the state of $G_{IIa} = 0$ and $G_{IIa} = G_{IIc}$. The layered G_I-G_{II} scatter diagram of specimens with different moisture contents under different temperature conditions is shown in Figure 8.

By comparing these figures, it can be found that in the dry state, whether at room temperature of 30°C or high temperature of 120°C, the dispersion of measured data is very small, and the envelope characteristics of delamination

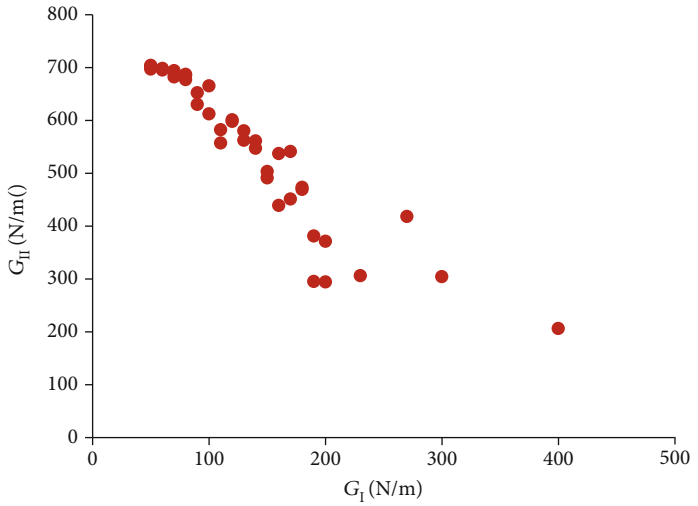

(a) G_I-G_{II} diagram of the dry specimen at 30°C

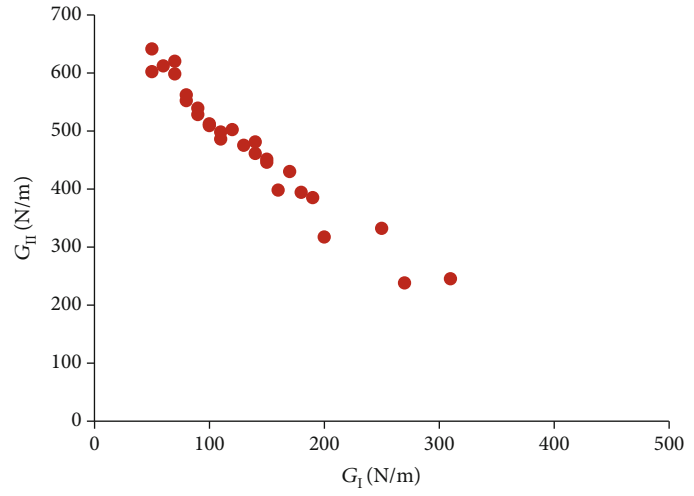

(b) G_I-G_{II} diagram of the dry specimen at 120°C

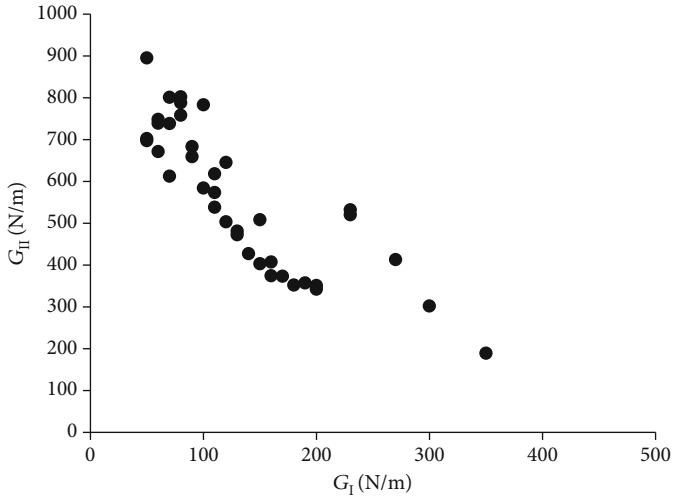

(c) G_I-G_{II} diagram of the high-moisture absorption specimen at 30°C

Figure 8: Continued.

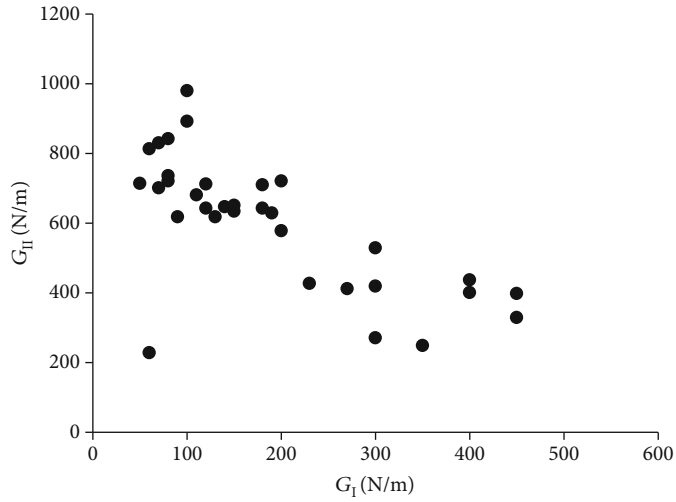

(d) G_I-G_{II} diagram of the high-moisture absorption specimen at 120°C

Figure 8: G_I-G_{II} scatter diagram under different conditions.

failure are obvious. Except G_{Ic}, other points are basically in a straight line. Therefore, it can be determined that the delamination criteria of composite unidirectional plates in the dry state are straight lines. However, G_{Ic} is not on this straight line, which shows that there are inconsistencies between the calculation formula of pure type I and that of type I stratification in mixed stratification. In particular, the value of G_{Im} is larger than that of G_{Ic}. This is difficult to explain from the perspective of energy.

4.2. Durability Test. The relative strength of the composites after aging at 95°C and heat was 88%. However, the humid and hot environment will have a great impact on the resin matrix and interface. The change of the resin matrix or interface properties will change its failure mechanism and failure mode and affect the longitudinal tensile strength. For brittle resin or carbon fiber composites with a strong interface, the mild liquid and thermal environment can increase their longitudinal tensile strength. For the flexible resin or weak interface, the liquid and thermal environment will reduce the strength. It can be seen from Table 3 that liquid heat has little effect on the longitudinal strength and measurement of unidirectional composite carbon fiber. For unidirectional glass fiber composites, the tensile strength decreases significantly because the glass fiber is corroded by the liquid and thermal environment. The surface treatment of glass fiber and its combination with resin directly affect the effect of protecting glass fiber from water corrosion, which has a great impact on the tensile strength of glass fiber composites.

Because the warm and humid environment will lead to the softening of the resin matrix, when the resin matrix softens, its coefficient will be significantly reduced. This will significantly reduce the longitudinal compressive strength of unidirectional composites, and the performance will degenerate into nonlinearity. Under high temperature and humidity, the compressive strength decreases, but the compressive strength under room temperature and humidity is basically unchanged. With the increase in temperature, the hygroscopicity increases, and the strength and coefficient decrease significantly. It can be seen from Table 3 that the longitudinal compressive strength of unidirectional composites at 120°C and 1.00% moisture absorption is 29.53% lower than that at 20°C and 0.50% moisture absorption. Due to the high moisture absorption of aramid fiber, the longitudinal compressive strength of unidirectional aramid composite fiber will be significantly reduced in the humid and warm environment [24, 25].

4.3. Accumulation of Mechanical Property Degradation. The hygroscopic environment of composites is constantly changing. When the hygroscopic environment conditions change, the hygroscopic characteristics of composites also change. The mechanical properties will further change on the basis of the influence of the previous wet and hot environment, and the changes in properties will accumulate. In this process, the mechanical properties of the material may be reduced or partially recovered under wet and hot conditions. As shown in Figure 9(a), the performance of the composite decreases after time Δt_1 in humid and hot environment 1. In the process of time Δt_2, the mechanical properties of the composites recovered due to the decrease in moisture absorption or the change in temperature.

As the hygroscopic characteristics of the materials will change after the change in the humid and hot environment, the change law of the mechanical properties of the composites will also change. Therefore, this paper adopts the equivalent of the performance degradation amount. As shown in Figure 9(b), it is assumed that the performance degradation amount of composite material after time Δt_1 is equal to the performance degradation amount after time t_{21} under humid and hot environment 1.

Table 3: Effect of damp-heat conditions on the resistance of composites.

Moisture absorption (%)	Temperature (%°C)	E_x (GPa)	E_y (GPa)	X' (MPa)	X (MPa)	Y (MPa)	Y' (MPa)	S (MPa)
0.50	-30	183	10.60	1510	1507	42	261	71
0.50	20	180	10.10	1490	1490	38	244	66
1.00	120	168	7.60	1402	1050	26	167	45

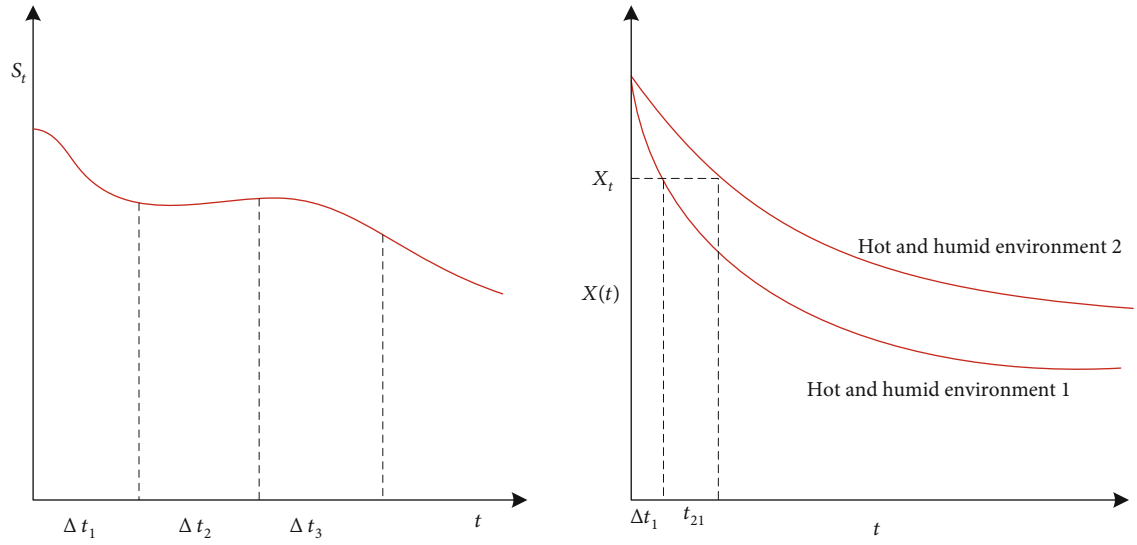

(a) Accumulation of degradation of damp-heat aging performance

(b) Equivalent relationship of performance degradation

Figure 9: Mechanical property degradation data.

5. Discussion

Firstly, through the study of relevant knowledge points of literature works, this paper has preliminarily mastered the relevant basic knowledge. This paper analyzes how to study the interlaminar fracture toughness and durability of composites in the humid and hot environment. This paper expounds on the concept and related methods of interlaminar fracture toughness, explores the composites in the humid and hot environment, and analyzes the interlaminar fracture toughness and durability through experiments.

After absorbing water, the mechanical properties of polymer matrix composites will change. The mechanical properties of liquid will also change due to the change in moisture absorption. Generally speaking, the axial properties of unidirectional composites are not greatly affected by moisture absorption, while the transverse and shear properties of materials are reduced due to the influence of the liquid and thermal environment on the matrix and interface [26]. When the moisture absorption reaches saturation, the hydrodynamic properties of the composites also tend to have a constant value.

The experimental analysis shows that moisture absorption has no obvious effect on the breaking resistance of the material at room temperature. At high temperatures, moisture absorption will increase the dimensional hardness of the composites. The temperature has the least effect on the mixed dimension fracture hardness of the dry sample, and the moisture absorption of the sample is relatively high. When the temperature is lower than 60°C, the hardness changes slightly. When the temperature is higher than 60°C, the hardness increases with the increase in temperature. Through the microfracture analysis, it is found that the single action of moisture absorption or high temperature makes the matrix toughness enhanced, and the fracture presents a ductile fracture morphology. The two work together to enhance the viscosity of the resin matrix.

6. Conclusion

Because polymers will age under the influence of external environmental factors, moisture and heat are the most important factors leading to the aging of composites. Therefore, the design and use departments in this paper pay special attention to the possible damage and mechanical properties of such composites in the humid and warm environment, which is an important guarantee and premise to promote their reasonable and effective implementation. The research on wet aging of composites is a research topic with theoretical and practical significance. Although some progress has been made, its important role in guiding practical engineering applications still needs to be further studied. The work of this paper is only a preliminary exploration, and there are still many topics that need further research.

Data Availability

No data were used to support this study.

Conflicts of Interest

The authors declare that there is no conflict of interest with any financial organizations regarding the material reported in this manuscript.

References

[1] B. Gao, X. Ning, and P. Xing, "Shock wave induced nanocrystallization during the high current pulsed electron beam process and its effect on mechanical properties," *Materials Letters*, vol. 237, no. 15, pp. 180–184, 2019.

[2] X. Zhang, Z. Li, X. Wang, and J. Yu, "The fractional Kelvin-Voigt model for circumferential guided waves in a viscoelastic FGM hollow cylinder," *Applied Mathematical Modelling*, vol. 89, pp. 299–313, 2021.

[3] L. Zhang, Y. Liu, G. Sang, and Y. Zhai, "Heat & moisture comprehensive property for lime-slag/soil composites based on response surface methodology," *Acta Materiae Compositae Sinica*, vol. 34, no. 5, pp. 1095–1102, 2017.

[4] Z. Zong, L. Yang, H. Zhang, and L. Xiong, "Preparation of environment coordination Ce-La/TiO_2 composites and photocatalytic-moisture-heat properties," *Cailiao Gongcheng/Journal of Materials Engineering*, vol. 46, no. 5, pp. 145–150, 2018.

[5] S. Kasaragadda, I. M. Alarifi, M. Rahimi-Gorji, and R. Asmatulu, "Investigating the effects of surface superhydrophobicity on moisture ingression of nanofiber-reinforced bio-composite structures," *Microsystem Technologies*, vol. 26, no. 2, pp. 447–459, 2020.

[6] W. Yu, G. Zhang, C. Liu, and S. Fan, "Hard carbon nanotube sponges for highly efficient cooling *via* moisture absorption–desorption process," *ACS Nano*, vol. 14, no. 10, pp. 14091–14099, 2020.

[7] K. Tanaka, N. Hosoo, and T. Katayama, "Effects of temperature on the fiber matrix interfacial properties of carbon fiber reinforced highly heat resistant polyamide resin," *Journal of the Society of Materials Science Japan*, vol. 66, no. 10, pp. 746–751, 2017.

[8] Y. Liu, S. Jiang, W. Yan, J. Qin, and J. Yu, "Enhanced thermal property and anti-moisture absorption of PA6/P (*N*-(4-carboxyphenyl)maleimide-alt-triallyl isocyanurate) composites based on solid-state interfacial reaction," *Journal of Materials Research and Technology*, vol. 9, no. 5, pp. 11291–11302, 2020.

[9] Y. Chen, X. Xiong, and Q. Gao, "Digestibility and physicochemical properties of starch-galactomannan complexes by heat-moisture treatment," *Food Hydrocolloids*, vol. 77, pp. 853–862, 2018.

[10] X. Han, L. Yuan, A. Gu, and G. Liang, "Development and mechanism of ultralow dielectric loss and toughened bismaleimide resins with high heat and moisture resistance based on unique amino-functionalized metal-organic frameworks," *Composites Part B Engineering*, vol. 132, pp. 28–34, 2018.

[11] Y. Su, J. Li, and X. Zhang, "A coupled model for heat and moisture transport simulation in porous materials exposed to thermal radiation," *Transport in Porous Media*, vol. 131, no. 2, pp. 381–397, 2020.

[12] W. Peng, Y. Tao, L. Ziqiang et al., "A superhydrophobic/electrothermal synergistically anti-icing strategy based on graphene composite," *Composites Science and Technology*, vol. 198, article 108307, 2020.

[13] A. A. Dalinkevich, T. A. Nenasheva, and I. G. Kalinina, "The role of interfacial effects in hydrothermal aging of aramid composites," *Protection of Metals and Physical Chemistry of Surfaces*, vol. 57, no. 2, pp. 352–360, 2021.

[14] L. Calabrese, L. Bonaccorsi, P. Bruzzaniti, E. Proverbio, and A. Freni, "SAPO-34 based zeolite coatings for adsorption heat pumps," *Energy*, vol. 187, article 115981, 2019.

[15] A. Purohit and A. Satapathy, "Dry sliding wear characteristics of epoxy composites filled with steel industry slag and sludge particles: a comparative study," *Materials Today Proceedings*, vol. 5, no. 5, pp. 11906–11913, 2018.

[16] I. Ahmadi, "Evaluation of effective thermal diffusivity and conductivity of fibrous materials through computational micromechanics," *Heat & Mass Transfer*, vol. 53, no. 1, pp. 277–290, 2017.

[17] D. Aydin, S. P. Casey, X. Chen, and S. Riffat, "Numerical and experimental analysis of a novel heat pump driven sorption storage heater," *Applied Energy*, vol. 211, pp. 954–974, 2018.

[18] R. Panduro and J. L. Mantari, "Hygro-thermo-mechanical behavior of classical composites," *Ocean Engineering*, vol. 137, pp. 224–240, 2017.

[19] T. R. Rigolin, M. C. Takahashi, D. L. Kondo, and S. H. P. Bettini, "Compatibilizer acidity in coir-reinforced PLA composites: matrix degradation and composite properties," *Journal of Polymers and the Environment*, vol. 27, no. 5, pp. 1096–1104, 2019.

[20] Y. Chen, D. Li, X. Q. Xie, Y. Gao, and Y. L. He, "Theoretical modeling and experimental validation for the effective thermal conductivity of moist silica aerogel," *International Journal of Heat and Mass Transfer*, vol. 147, article 118842, 2020.

[21] W. Liu, W. Xi, R. Hu et al., "Preparation and characterization of sodium silicate/epoxy resin composite bonded Nd-Fe-B magnets with high performance," *Journal of Rare Earths*, vol. 37, no. 10, pp. 1083–1087, 2019.

[22] N. Banik, V. Dey, and G. Sastry, "An overview of lignin & hemicellulose effect upon biodegradable bamboo fiber composites due to moisture," *Materials Today Proceedings*, vol. 4, no. 2, pp. 3222–3232, 2017.

[23] F. Zhang, Z. F. Shi, Z. Z. Ma et al., "Silica coating enhances the stability of inorganic perovskite nanocrystals for efficient and stable down-conversion in white light-emitting devices," *Nanoscale*, vol. 10, no. 43, pp. 20131–20139, 2018.

[24] J. B. Alvey, J. Patel, and L. D. Stephenson, "Experimental study on the effects of humidity and temperature on aerogel composite and foam insulations," *Energy and Buildings*, vol. 144, pp. 358–371, 2017.

[25] Z. Candan, S. M. Shaler, J. P. Heller, and R. Edgar, "Enhancing dimensional stability of oriented strand composites within biorefinery," *Maderas Ciencia Y Tecnología*, vol. 19, no. 3, pp. 387–398, 2017.

[26] A. Y. Shaulov, R. A. Sakovich, E. M. Nechvolodova et al., "The modification of poly (metal phosphates) by pentaerythritol," *Polymer Science, Series B*, vol. 62, no. 5, pp. 534–539, 2020.